Journal of
MARINE RESEARCH

Bottom water variability in the Samoa Passage

by Gregory C. Johnson[1], Daniel L. Rudnick[2] and Bruce A. Taft[1]

ABSTRACT

The Samoa Passage (near 10S, 170W) is the channel through which the coldest, saltiest, densest bottom water approaches the North Pacific Ocean from its southern source. Over the past 25 years, three hydrographic sections have been made across the passage. A section occupied in 1968 shows little sign of modified North Atlantic Deep Water (NADW) within the northward flowing Lower Circumpolar Water (LCPW). In contrast, a section occupied in 1987 shows a strong negative curvature in θ-S (potential temperature-salinity) and a local maximum in salinity characteristic of NADW. A third section occupied in 1992 reveals a marginal NADW signature. The three sections are objectively mapped and very fine-scale bivariate areal θ-S censuses are made for a quantitative comparison of differences in water-mass structure. The strength of the NADW signature could fluctuate over a wide range of time-scales. However, these data are consistent with decadal variability, with no NADW signal in the passage in 1968, a strong signal in 1987, and a weak one in 1992. The geostrophic volume transport through the passage is 1.0 ± 0.2, 5.6 ± 1.3, and $4.8 \pm 0.6 \times 10^6$ m^3 s^{-1} below a zero-velocity surface (ZVS) of $\theta = 1.2°$C for the 1968, 1987, and 1992 sections respectively. The transport estimates, made for comparison with those from velocity data presently being collected by a current meter array in the passage, are sensitive to variations in the choice of ZVS.

1. Introduction

The Samoa Passage is the primary channel through which Lower Circumpolar Water (LCPW) flows from the Southern Ocean into the North Pacific (Mantyla and Reid, 1983). The LCPW encompasses two cold, salty, (relatively) oxygen-rich, and

1. NOAA Pacific Marine Environmental Laboratory, Bin C15700/Bldg. 3, 7600 Sand Point Way N. E., Seattle, Washington, 98115-0070, U.S.A.
2. Scripps Institution of Oceanography 0230, University of California San Diego, La Jolla, California, 92093-0230, U.S.A.

(relatively) silica-poor water-masses. On the top is modified North Atlantic Deep Water (NADW; here defined as water of $0.7 < \theta \le 1.2°C$); warmer, saltier, more oxygen-poor, and more silica-poor. Below the NADW is colder, fresher, more oxygen-rich, and more silica-rich water that is too warm to be Antarctic Bottom Water, but shows its influence (modified AABW; here $\theta \le 0.7°C$). The local salinity maximum and silica minimum associated with NADW disappear north of the passage (Craig *et al.,* 1981; their Plates 5 and 13). Thus, the passage is the farthest point in the World Ocean to which the core of NADW, defined explicitly by these features, can be traced from its source before it is mixed away.

Flow through the passage was first systematically explored in June–July 1968 during the Styx expedition (Reid and Lonsdale, 1974). Hydrographic stations were occupied and current meters deployed for roughly two-day periods to determine the route of cold water in the region. The layer of strong stratification, with a maximum near potential temperature $\theta = 0.9°C$, was taken to be the boundary between northward flow of LCPW and southward flow of warmer, fresher, oxygen-poor, and silica-rich North Pacific Deep Water (NPDW; Sverdrup *et al.,* 1942; here $1.2 < \theta \le 2.0°C$). No estimates of transports through the passage were presented. The passage is the only route into the North Pacific for water of $\theta \le 0.8°C$ (Mantyla and Reid, 1983).

The first modern CTD section across the passage was occupied in June 1987 during the TEW expedition (Taft *et al.,* 1991). These measurements clearly show a break in slope of the θ-S curve toward higher salinities below $\theta \approx 1.2°C$, negative curvature in θ-S below the break, and a deep local salinity maximum, all features characteristic of NADW. This break occurs just above the stratification maximum. Since this NADW signature must be coming from the south, the break in θ-S suggests a zero-velocity surface (ZVS) above the stratification maximum, rather than in it as suggested by Reid and Lonsdale (1974). Using this break ($\theta = 1.17°C$) as their ZVS, Taft *et al.* (1991) estimated a net northward volume transport of 6.0 ± 1.1 Sv (1 Sv $= 1 \times 10^6$ m^3 s^{-1}) of LCPW below the ZVS, extrapolating the velocity at the deepest common level of each station pair to the area below. Their error estimate for the transport is a lower bound, gained from calculating transports using a narrow ($\pm 0.05°C$) range of θ-surfaces determined from the data as ZVSs and considering the extrapolated velocities as a source of error.

A CTD section across the passage was occupied in September 1992 during the deployment of an array of current meter moorings in the passage to measure the deep flow there (WOCE PCM11; U.S. WOCE Implementation Plan, 1992; Rudnick, 1992). The three sections across the passage are objectively mapped. Very fine-scale bivariate areal θ-S censuses show quantitatively that the salinity signal of NADW clearly visible across the passage in 1987 was absent in 1968 and weak in 1992. The mapped data are used to make geostrophic estimates of the transport of deep water through the passage for each section. The formal errors in transport are calculated and the effect of varying the ZVS is explored.
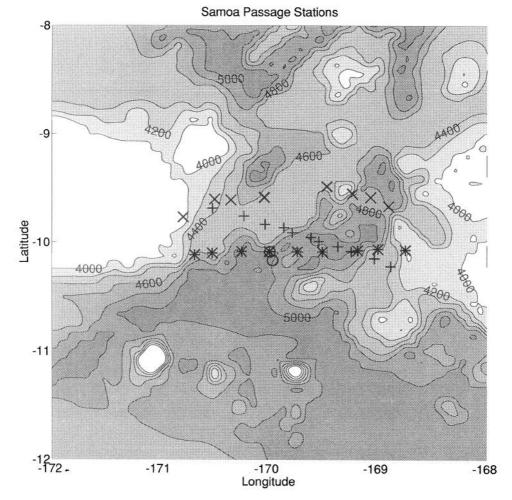
Samoa Passage Stations

Figure 1. Station locations (Table 1) from Styx (x's), GEOSECS (o), TEW (*'s), CGC-90-MB (o), and PCM11 (+'s), with 4000 m to 5000 m isobaths contoured at 200 m intervals from the ETOPO5 digital bathymetric data set. The Styx, TEW, and PCM11 sections span the Samoa Passage. GEOSECS sta. 257, CGC-90-MB sta. 55, and TEW sta. 28 are within 10 km of one another.

2. Data

Deep salinity variations within the Samoa Passage are small. The maximum range of salinity within or among cruises at a constant θ (for $\theta \le 1.2°C$) is 0.010 psu. Relatively small discrepancies have been found between salinity values calculated from the label on a given standard seawater (SSW) batch and those measured with a salinometer when many different SSW batches are analyzed at once and compared (Mantyla, 1987). Five different data sets are discussed (Fig. 1; Table 1), each of which was standardized using a different batch of SSW. To best compare these data, salinity

Table 1. Expeditions, Dates, Station(s), SSW batch, and SSW offset (Mantyla, 1987) applied
   to the data. The three most recent data sets are comprised of CTD data. No offset is applied
   to CGC-90-MB or PCM11 data because none has been determined for the relevant SSW
   batches. Recent SSW batches have had negligible offsets (Mantyla, personal communica-
   tion), so this action may be appropriate.

Expedition	Date	Station(s)	SSW Batch	SSW Offset (psu)
Styx*	Jun–Jul 1968	15, 17, 31–34, 41	p47	0.000
GEOSECS*	Jan 1974	257	p58	+0.002**
TEW	Jun 1987	23–31	p90	−0.002
CGC-90-MB	Apr 1990	55	p112	0.000
PCM11	Sep 1992	2–12	p120	0.000

*Bottle Data
**The GEOSECS salinities have been adjusted by an additional +0.002 psu in Figure 3.

offsets from Mantyla (1987) are applied to correct for these SSW batch discrepancies
when available (Table 1), reducing differences among the deep θ-S relations.

   Three hydrographic sections spanning the passage are compared (Fig. 1; Table 1).
Eight stations from the Styx expedition (Scripps Institution of Oceanography, 1971)
comprise a Nansen bottle section across the passage at roughly 9.5S with a mean
station spacing of 31 km (64 km maximum). This section is north of one in the Samoa
Basin from that expedition previously published (Reid and Lonsdale, 1974, their
Figs. 4 and 8). Nine stations from the TEW expedition (Mangum *et al.*, 1991)
comprise a CTD section across the passage at 10S (50 km south of the Styx section)
with a mean station spacing of 27 km (35 km maximum). Another CTD section,
consisting of eleven PCM11 stations (Rudnick, 1992), spans the passage starting at
9.5S in the west and ending at 10S in the east, with a mean spacing of 19 km (33 km
maximum). All three sections approach the 4000 and 4200 m isobaths on the west
and east sides of the passage respectively (Fig. 1), encompassing the water of $\theta \leq$
0.8°C at this latitude (Mantyla and Reid, 1983).

   The pressures, temperatures, and salinities from these sections are used to
calculate potential temperature, depth, specific-volume anomaly, and buoyancy
frequency (N). N is calculated from the slope of a three-point fit of density
referenced to the pressure of the central point against depth (the top and bottom
points from a two-point fit). Objective maps of these quantities are made for each
section, for the purposes of contouring, comparison, transport calculations, and
formal error estimates (Bretherton *et al.*, 1976). The mapping procedure explicitly
accounts for errors in transport calculations resulting from extrapolating geostrophic
velocities below the deepest common level of station pairs (Roemmich, 1983). Maps
for all three sections are made using 0.05 for the ratio of measurement noise to signal
energy. For the two CTD sections, the 2 dbar CTD data are averaged in 50 dbar bins,
with the data below the deepest full bin averaged in a smaller bin. Maps are made
with 6–7 km horizontal spacing and 25 m vertical spacing using a Gaussian covari-

ance with 40 km lateral and 100 m vertical correlation lengths. These correlation lengths are half those estimated from the PCM11 temperature data, and were chosen to minimize distortion of the θ-S characteristics while keeping formal errors relatively small between stations. For the Nansen bottle data both correlation lengths were increased by a factor of three, owing to the large station spacing and the average 200 to 400 m vertical spacing between bottles. This resulted in some smoothing of the data, which were slightly noisier than the CTD data.

In January 1974 GEOSECS sta. 257 (Broecker *et al.*, 1982) was occupied within 10 km of TEW sta. 28 (Fig. 1). In April 1990 CGC-90-MB sta. 55 was occupied within 2 km of TEW sta. 28 (McTaggart *et al.*, 1993). These three stations are compared to gain further insight into temporal variability of NADW in the region.

3. θ-S comparisons

The water-masses of concern are LCPW (θ ≤ 1.2°C), the cold and salty bottom water from the south, and NPDW (1.2 < θ ≤ 2.0°C), the warmer and fresher deep water from the north. NADW can be identified by a local salinity maximum within the LCPW that can extend as far north as the Samoa Passage. This definition is expanded to encompass the negative curvature in θ-S (0.7 < θ ≤ 1.2°C; referred to as the NADW θ-classes) that is sometimes present in the passage. (Hence the modified AABW θ-classes have θ ≤ 0.7°C.) The temporal variability of this NADW signature within the passage is quantified.

The objectively mapped data with an estimation error less than 0.1 of the signal energy (to assure that θ-S characteristics are preserved) are used for bivariate areal θ-S censuses (two-dimensional versions of those in Worthington, 1981). These maps comprise 99, 90, and 99% of the cross-sectional area for θ ≤ 1.5°C for the Styx, TEW, and PCM11 sections respectively. The θ-classes extend from 0.5 to 1.5°C in 0.02°C intervals (five times finer than Worthington, 1981). The S-classes extend from 34.67 to 34.72 psu in 0.001 psu intervals (ten times finer than Worthington, 1981). The areas are shaded with a logarithmic scale (Fig. 2) to accentuate variations among censuses within the NADW θ-classes. This scale is used because water in the NADW θ-classes is highly stratified (see Section 4). Thus NADW occupies a relatively small amount of the cross-sectional area of the passage. The S-class with the most area in a single θ-class is referred to as the salinity mode.

The salinity data from the Styx expedition are noisier than those from the later expeditions. For the eight stations used, there are 20 bottles reported in the coldest (θ ≤ 0.7°C) water in the passage. Their mean salinity is 34.711 psu, with a standard deviation of 0.0025 psu and a range of 0.008 psu. The station and bottle spacing make long correlation lengths necessary (tending to smooth out some of the variability). There is a faint hint of negative curvature in the salinity modes near θ ≈ 0.82°C (Fig. 2a). However, the saltiest salinity mode is near the bottom. The noise in the salinity measurements and the vertical bottle spacing (with usually only two bottles
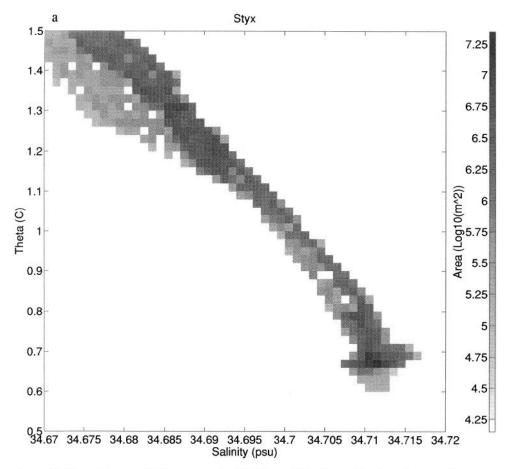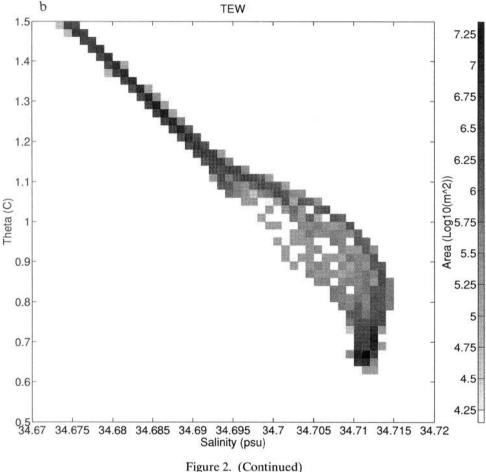
Figure 2.- Bivariate areal θ-*S* censuses in 0.02°C and 0.001 psu θ and *S*-classes. The areal shading scale is logarithmic to accentuate differences in the NADW θ-classes. (a) The Styx census is somewhat noisy but a NADW signature is absent. (b) The TEW census reveals a strong NADW signature with a local salinity maximum. (c) The PCM11 census resembles the Styx census more than the TEW census, with only a weak NADW signal.

per station in the NADW θ-classes) makes picking out the salinity signature of NADW within the LCPW, even as a negative curvature in salinity modes, problematic.

The TEW data group very tightly above and below the NADW θ-classes (Fig. 2b). Despite the noise in the individual Styx measurements, the coldest salinity modes of the two censuses (θ ≤ 0.7°C), agree to within 0.002 psu, demonstrating remarkable consistency. Unlike the Styx census, the salinity modes in the NADW θ-classes show a prominent negative curvature and a local maximum. The salinity modes within the NADW θ-classes are as much as 0.007 psu higher in the TEW census compared to those in the Styx census.

Figure 2. (Continued)

The PCM11 data (Fig. 2c) group fairly tightly above and below the NADW θ-classes, matching corresponding salinity modes from the TEW census to within 0.001 psu. All three data sets have salinity modes that agree to within 0.002 psu in the coldest (modified AABW) θ-classes. However, within the NADW θ-classes, most of the PCM11 census looks more like the Styx census than the TEW census, with little negative curvature in the salinity modes, and the maximum salinity mode near the bottom. The difference of salinity modes within a given NADW θ-class is as great as 0.008 psu between the TEW and PCM11 censuses.

These three censuses suggest a strong NADW signature within the passage in 1987, no discernable signal in 1968, and a weak one in 1992. Single stations occupied near TEW sta. 28 are compared with it further to explore temporal variability (Fig. 3). GEOSECS sta. 257 salinities are shifted by +0.002 psu above the adjustment suggested by Mantyla (1987) to overlay the others outside the NADW (Table 1;
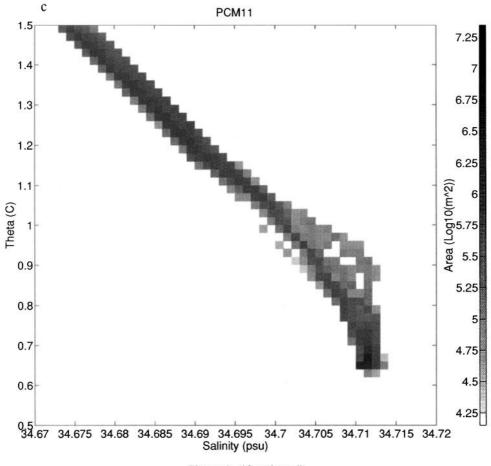
Figure 2. (Continued)

Fig. 3). With this shift all three stations overlay in the presumably stationary modified AABW. The curves diverge in the NADW above the salinity maximum. The GEOSECS station is as much as 0.007 psu fresher than the TEW station. Similarly, CGC-90-MB sta. 55 is as much as 0.004 psu fresher than the TEW station. However, all three stations show negative curvature and a salinity maximum above the bottom.

Taken together, the measurements suggest that the NADW salinity signature within the Samoa Passage was absent in 1968, moderate in 1974, strong in 1987, moderate in 1990, and weak in 1992. The single stations in 1974 and 1990 are probably not representative of conditions across the entire passage in those years. The section data show the NADW signature stronger toward the west side of the passage. Comparisons among the single stations depend on the assumption that this overall spatial pattern of the NADW signature in the passage is steady and only the amplitude of the signature varies. With this strong assumption, the data are consis-
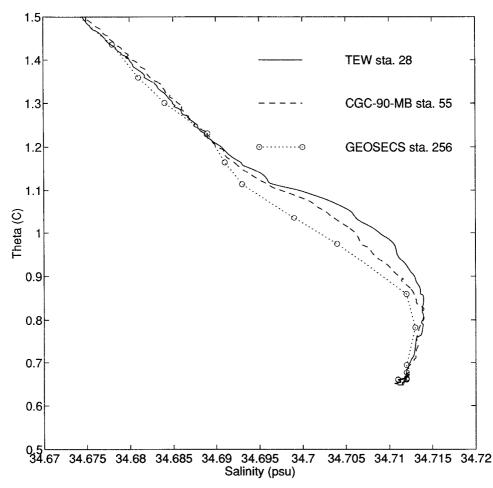
Figure 3. θ-*S* curves for TEW sta. 28 (solid line), CGC-90-MB sta. 55 (dashed line), and GEOSECS sta. 257 (dotted line, o's at bottle locations). GEOSECS and CGC-90-MB curves are as much as 0.007 and 0.004 psu fresher than the TEW curve above the local salinity maximum, respectively.

tent with decadal variability of the NADW signature. Of course, the signal could vary over much shorter time-scales.

4. Buoyancy frequency

As mentioned in the previous section, the θ-classes in which the NADW signature exists are associated with a maximum in stratification, presented in terms of buoyancy frequency (*N*; Fig. 4). For all three sections *N* decreases from 2000 m depth to θ ≈ 1.2°C, then increases to a maximum in the NADW θ-classes. It then decreases to very low values in the modified AABW θ-classes. The vertical sections show that
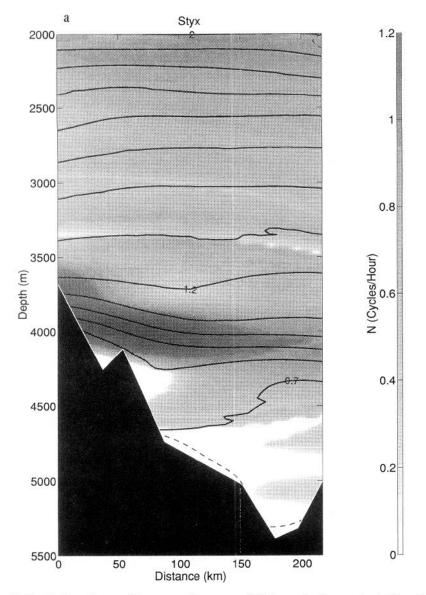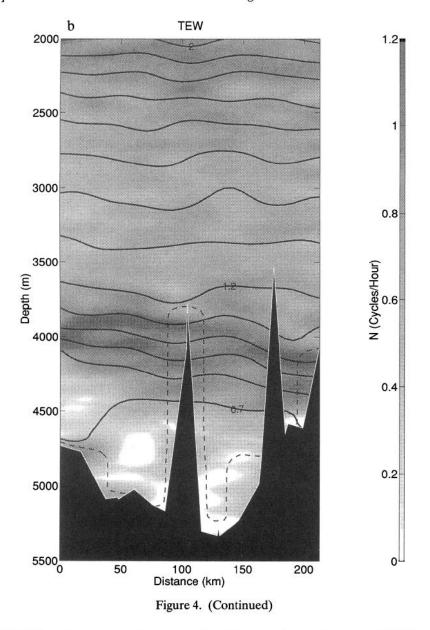
Figure 4. Vertical sections of buoyancy frequency (*N,* in cycles/hour, shaded), potential temperature (θ, in °C, solid lines), and the 0.10 contour of the ratio of estimation error to signal energy (dashed lines) across the Samoa Passage. Potential isotherms bounding the NPDW, NADW, and modified AABW θ-classes are labeled. A local *N* maximum is found within the NADW θ-classes. Differences in bottom roughness among the sections are owing to differences in measurement resolution. Vertical exaggeration is 125:1. (a) Styx section. (b) TEW section. (c) PCM11 section.

Figure 4. (Continued)

the NADW θ-classes comprise about ⅔ of the areal extent of the LCPW in the passage and the modified AABW θ-classes make up the remaining ⅓. This feature is reflected in the bivariate θ-S areal censuses (Fig. 2). However, it is not apparent in simple θ-S curves, which show that NADW extends over a θ-range eight times that of the modified AABW (Fig. 3).
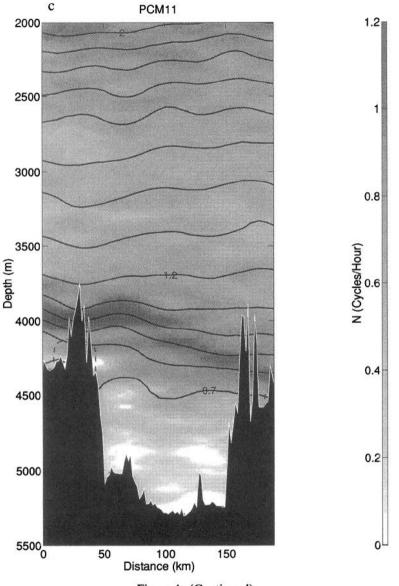
Figure 4. (Continued)

Reid and Lonsdale (1974) suggested that the N maximum is the signature of a boundary between northward flowing LCPW and southward flowing NPDW. Since isopycnals in the boundary generally slope upward toward the west, velocity is increasingly northward toward the bottom in the high N region. By their reasoning, the ZVS for geostrophic calculations was placed near the N maximum so that the water below it moved north and that above it moved south at roughly equal velocities.

However, negative curvature in θ-S below θ ≈ 1.2°C suggests that NADW is associated with the N maximum. Thus the ZVS should be placed higher to assure that all of the NADW moves northward, away from its source, along with the colder water below (Taft *et al.*, 1991).

The northward flow of LCPW in the Samoa Passage is a continuation of the northward flowing Deep Western Boundary Current (DWBC) observed offshore of New Zealand and the Tonga-Kermadec Ridge at 43 and 28S in the Pacific Ocean (Warren, 1973). The DWBC consists of dense water formed in the polar regions. Thus it might be thought of simply as a dense gravity current travelling away from its source (banked against the western boundary because of the Earth's rotation). Density-driven plumes often have a bottom layer that is well mixed (for this current, the modified AABW), and a stratified cap (the NADW), as in Turner (1973). In these gravity currents, most of the water in this stratified region moves along with the plume. Thus this simple plume model of the DWBC suggests that the ZVS should be placed above the N maximum, not in it.

5. Transport estimates

We have shown that the negative θ-S curvature in the NADW and the increase in N both begin just below θ ≈ 1.2°C in the Samoa Passage. While there is some eddy signal present in the geostrophic velocity field with the correlation lengths used to make the maps, the velocity is for the most part increasingly northward below θ ≈ 1.2°C (Fig. 5). By the arguments above, the best choice for a ZVS is at θ = 1.2°C. This ZVS is shallower than that inferred by Reid and Lonsdale (1974) from the Styx data, but very similar to that used by Taft *et al.* (1991) for the TEW data (see their Fig. 7 for the TEW velocity section across the passage). Below the ZVS (in the LCPW; θ ≤ 1.2°C) the net transports are 1.0 ± 0.2, 5.6 ± 1.3, and 4.8 ± 0.6 Sv (positive northward, with formal standard deviations from the objective analysis) for the Styx, TEW, and PCM11 sections respectively.

The Styx data are probably not adequate for transport estimates in the LCPW since the salinities are noisy, the sampling is relatively sparse, and the bottom bottles range from 44 to 220 m above the bottom. The formal Styx errors are artificially small because the mapping correlation lengths are three times longer than those used for the CTD sections. Using the shorter correlation lengths the Styx LCPW transport (below the ZVS) is estimated to be 2.1 ± 0.9 Sv. The two CTD sections yield larger, more significant, LCPW transports (below the ZVS) that agree to well within the formal error estimates. These error estimates are large, since the correlation lengths used are half those suggested by the data. Doubling the correlation lengths for the CTD section maps smooths eddies in the velocity fields, reduces formal errors, and slightly increases net northward and southward transports. However, the smoothing also visibly distorts the θ-S properties when the maps are compared with individual
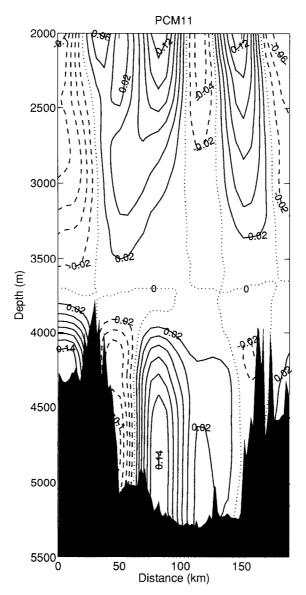
Figure 5. Vertical section of geostrophic velocity (v, in m s^{-1}) normal to the PCM11 section contoured at 0.02 m s^{-1} intervals. The ZVS is $\theta = 1.2°C$. Positive (northward) velocities are solid lines, negative (southward) velocities are dashed, and the zero contour is dotted. Flow is predominantly increasingly northward with increasing depth below the ZVS (in the LCPW). Vertical exaggeration is 125:1.

Table 2. Net geostrophic transports (in Sv, 1 Sv = 1 × 10^6 m^3 s^{-1}) for three water masses defined by the θ-classes listed from the three sections using the objective maps. Formal standard deviations are derived from the objective analysis (see text). The NADW and the modified AABW make up the LCPW.

			Expedition	
Water Mass	θ-Classes	Styx	TEW	PCM11
NPDW	1.2 < θ ≤ 2.0°C	+4.8 ± 0.7	−2.1 ± 0.3	+3.5 ± 0.4
NADW	0.7 < θ ≤ 1.2°C	+1.8 ± 0.2	+2.9 ± 0.7	+1.8 ± 0.3
AABW	θ ≤ 0.7°C	−0.8 ± 0.2	+2.6 ± 0.8	+2.9 ± 0.4

station data. Increases in transport are not significant, and the maps that preserve the data are preferable.

When the transport is broken down into θ-classes for NPDW (1.2 < θ ≤ 2.0°C), NADW (0.7 < θ ≤ 1.2°C), and modified AABW (θ ≤ 0.7°C), differences among the sections become clearer (Table 2). For the two CTD sections, transports in the modified AABW θ-classes agree to well within error estimates. However, PCM11, with its weak NADW signature, has a transport in the NADW θ-classes about 60% that of TEW. This difference exceeds even the large formal errors. The TEW NPDW transport is southward, whereas the PCM11 NPDW transport is northward, toward the source. Assuming the ZVS is reasonable, this difference may exist because NPDW is not restricted to the passage, and the location of its southward flow may vary in time.

Using ZVSs of θ = 0.7, 1.2, and 2.0°C demonstrates the sensitivity of LCPW transport to the choice of ZVS (Table 3). Summing the transports in 0.1°C bins shows the mean shear across the passage (Fig. 6). The Styx section has the most complicated response to changes in the ZVS, but is probably undersampled. The TEW section has nearly monotonic shear. Raising the ZVS to θ = 2.0°C has water moving northward throughout the section, while lowering it to 0.7°C has water moving southward everywhere. However, the shear across the PCM11 section is such that raising the ZVS to θ = 2.0°C has water moving southward everywhere, and lowering it to 0.7°C also has water moving southward everywhere. In fact, the maximum northward transport of LCPW using a θ-surface ZVS for PCM11 is for θ = 1.2°C. This differing sensitivity of the two CTD sections to shifts in the ZVS is interesting since the 2000 dbar (close to θ = 2.0°C) ZVS used farther south (Warren, 1973) yields wildly different estimates of LCPW transport for the two sections in the passage.

The net transports across the sections vary somewhat from occupation to occupation. Discounting the Styx transport, the two CTD sections give a northward transport of 5.2 ± 0.7 Sv of LCPW (below the ZVS of θ = 1.2°C) through the Samoa Passage. The reduction in transport in 1992 compared with 1987 is in the NADW. The NADW θ-S signature is also weaker in 1992 than in 1987. Transport above this ZVS changes sign in the two sections, with NPDW apparently flowing back toward its

Table 3. Volume transport (in Sv, 1 Sv = 1 × 10^6 m^3 s^{-1}) of LCPW ($\theta \leq 1.2°$C) for the Styx, TEW, and PCM11 sections for ZVSs at θ = 2.0, 1.2, and 0.7°C. Transports are calculated using the objective maps. Formal standard deviations are derived from the objective analysis.

		Expedition	
ZVS (θ)	Styx	TEW	PCM11
2.0°C	+2.7 ± 0.4	+8.6 ± 1.4	−2.7 ± 0.3
1.2°C	+1.0 ± 0.2	+5.6 ± 1.3	+4.8 ± 0.6
0.7°C	−1.5 ± 0.7	−3.6 ± 1.7	−2.8 ± 0.7

source in 1992. Neither of these changes are conclusive evidence of changes in net transport of NADW or NPDW, because, while the water of $\theta \leq 0.8°$C is constrained by the bathymetry to flow through the passage (Mantyla and Reid, 1983), there are other possible routes for water warmer than this.

6. Discussion

NADW can (sometimes) be traced as a local salinity maximum in the South Pacific as far north as the Samoa Passage (Fig. 1). Bivariate areal θ-S censuses and individual θ-S curves from short sections and individual stations in the passage show no NADW signal in 1968, a moderate signal in 1974, a strong one in 1987, a moderate one in 1990, and a weak one in 1992 (Figs. 2 and 3). A comparison between a pair of hydrographic sections taken across the Tasman Sea in 1967 and reoccupations in 1989–90 suggests that the volume of NADW in the Tasman Sea has increased at the expense of the volume of modified AABW (Bindoff and Church, 1992). However, while the NADW salinity signature in the Samoa Passage has varied over the past 25 years, the areas of the NADW and modified AABW θ-classes do not vary significantly among the censuses.

Four possible explanations for the variability in the Samoa Passage are advanced. Temporal variations in mixing along the path of the NADW may account for the variable NADW signal in the passage. Alternately, the water-mass property variations may be associated with transport variations in the NADW. These variations may also be owing to variability in the properties of the water-mass at its source in the North Atlantic. Finally, it is possible that the absence of NADW signature in the Styx data may be a result of being about 50 km downstream of the other sections. Horizontal intrusions with vertical scales of about 100 m within the NADW θ-classes in the passage are present in each CTD data set. Mixing may be sufficiently strong in the passage to obliterate the NADW signature over 50 km.

The local NADW salinity maximum (sometimes) present in the Samoa Passage is shallower, thicker, warmer, and saltier at 28S and more so at 43S (Warren, 1973). As the NADW moves north it is eroded, and the salinity maximum becomes deeper, thinner, colder, and fresher. This progression can also be seen in the CGC-90-MB
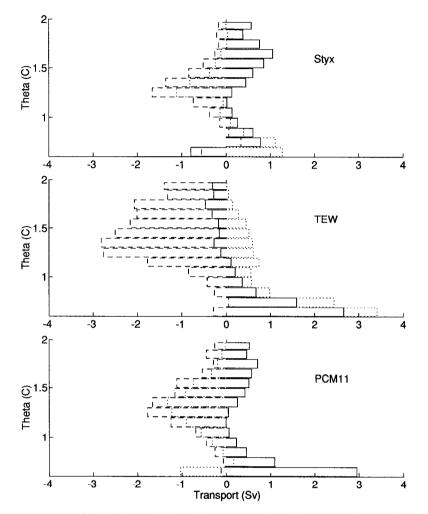
Figure 6. Transport for the Styx, TEW, and PCM11 sections (from top to bottom) summed in 0.1°C bins. Transports are calculated for ZVSs of $\theta = 0.7$°C (dashed lines), $\theta = 1.2$°C (solid lines) and $\theta = 2.0$°C (dotted lines). Shear is nearly monotonic for the TEW section, but changes sign near $\theta = 1.2$°C for the PCM11 section.

CTD data along 170W (McTaggart *et al.*, 1993). The N maximum associated with the NADW θ-classes in the passage (Fig. 4) becomes deeper, thinner, colder, and slightly stronger from south to north along 170W. This association may be the result of the NADW θ-classes being within the sheared, stratified cap of a cold, dense plume of water of southern origin flowing north. The N maximum appears to deepen and strengthen to the north as the NADW salinity signature weakens. North of the passage the salinity maximum is found at the bottom and the N maximum is absent; the NADW signatures have been mixed away.

Relating downstream changes of salinity and N in the synoptic section along 170W (following the DWBC's northward path) to temporal variations in the passage suggests that temporal variations in upstream mixing may account for changes in the NADW in the passage. The N maximum is stronger and occurs at a lower θ in 1968 and 1992 than in 1987, while the NADW salinity signal is strongest in 1987. Thus more mixing may have worked on the NADW found in the passage in 1968 and 1992 than that found there in 1987.

The reduction in NADW signature may be associated with a reduction of northward transport within the NADW θ-classes (Table 2). The weak NADW signature in 1992 compared to 1987 may be linked to the reduced northward transport in the NADW θ-classes. Were less NADW travelling north in the DWBC, the salinity maximum might be more vulnerable to mixing. However, the ZVS is constrained solely by water-mass arguments, and transports vary significantly with variations in the ZVS (Table 3; Fig. 6). In addition, the transport estimates may be temporally aliased by the eddies evident as θ-undulations in the passage (Fig. 4). The WOCE PCM11 current meter array is designed to yield a direct estimate of the transport below 4000 m in the passage, as well as its variability on time-scales shorter than about a year. The current meter array may also aid the choice of a ZVS in the passage.

A final speculation is that the variability of the NADW signature in the Samoa Passage may be owing to variability of NADW characteristics at the source. The NADW north of 50N freshened by about 0.020 psu between 1962 and 1981 (Brewer *et al.,* 1983). Saltier NADW was again observed in the North Atlantic in 1986 (Lazier, 1988). The 0.008 psu variations documented in the passage are smaller than these variations. The NADW is modified along its path from the North Atlantic to the passage (Reid and Lynn, 1971), so variations in the source are probably moderated by the mixing with various water masses. Variations in the properties of adjacent water-masses along the path of the NADW could similarly affect the NADW signature found in the passage. Extrapolation of the apparent mean speed of about 0.014 m s^{-1}, typically inferred from chlorofluorocarbon measurements in the deep component of NADW in the North Atlantic (Smethie, 1992), to the entire path of the NADW from the Norwegian Sea to the Samoa Passage given by Reid and Lynn (1971, their Fig. 9) suggests that variations in NADW characteristics at the passage could lag those at the source region by about a century. Unfortunately, the data available are inadequate to test this speculation.

calibrate the PCM11 CTD data. Contribution No. 1460 from NOAA's Pacific Marine Environmental Laboratory.

REFERENCES

Bindoff, N. L. and J. A. Church. 1992. Warming of the water column in the southwest Pacific Ocean. Nature, *357,* 59–62.

Bretherton, F. P., R. E. Davis and C. B. Fandry. 1976. A technique for objective analysis and design of oceanographic experiments applied in MODE-73. Deep-Sea Res., *23,* 559–582.

Brewer, P. G., W. S. Broecker, W. J. Jenkins, P. B. Rhines, C. G. Rooth, J. H. Swift, T. Takahashi and R. T. Williams. 1983. A climatic freshening of the deep Atlantic north of 50N over the past 20 years. Science, *222,* 1237–1239.

Broecker, W. S., D. W. Spencer and H. Craig. 1982. GEOSECS Pacific Expedition: Volume 3, Hydrographic Data 1973–1974. National Science Foundation, Washington D.C. 237 + xxvii pp.

Craig, H., W. S. Broecker and D. Spencer. 1981. GEOSECS Pacific Expedition: Volume 4, Sections and Profiles. National Science Foundation, Washington D.C., 251 + xiv pp.

Lazier, J. R. N. 1988. Temperature and salinity changes in the deep Labrador Sea, 1962–1986. Deep-Sea Res., *35,* 1247–1257.

Mangum, L., J. Lynch, K. McTaggart, L. Stratton and S. Hayes. 1991. CTD/O_2 Data Measurements Collected on TEW (Transport of Equatorial Waters) June–August 1987. Pacific Marine Environmental Laboratory, Seattle, Washington, NOAA Data Report ERL PMEL-33, 375 pp.

Mantyla, A. W. 1987. Standard Seawater comparisons updated. J. Phys. Oceanogr., *17,* 543–548.

Mantyla, A. W. and J. L. Reid. 1983. Abyssal characteristics of the World Ocean waters. Deep-Sea Res., *30,* 805–833.

McTaggart, K., D. Wilson and L. Mangum. 1993. CTD Measurements Collected on a Climate & Global Change Cruise Along 170W During February–April 1990. Pacific Marine Environmental Laboratory, Seattle, Washington, NOAA Data Report ERL PMEL-44, 265 pp.

Reid, J. L. and P. F. Lonsdale. 1974. On the flow of water through the Samoan Passage. J. Phys. Oceanogr., *4,* 58–73.

Reid, J. L. and R. J. Lynn. 1971. On the influence of the Norwegian-Greenland and Weddell seas on the bottom waters of the Indian and Pacific oceans. Deep-Sea Res., *18,* 1063–1088.

Roemmich, D. 1983. Optimal estimation of hydrographic station data and derived fields. J. Phys. Oceanogr., *13,* 1544–1549.

Rudnick, D. L. 1992. The Samoan Passage experiment: A component of the World Ocean Circulation Experiment current meter array PCM11. Cruise Report R. V. Knorr 138 leg 8, 15 September–27 September 1992. Unpublished Report, 10 pp.

Scripps Institution of Oceanography, University of California. 1971. Physical and Chemical data, Burton Island Expedition 28 February–15 April 1968 and Styx Expedition 4 April–4 August 1968. Unpublished Report, SIO Ref. 71–25, 62 pp.

Smethie, W. M. Jr. 1992. Tracing the thermohaline circulation in the western North Atlantic using chlorofluorocarbons. Prog. in Oceanogr., *31,* 51–99.

Sverdrup, H. U., M. W. Johnson and R. H. Fleming. 1942. The Oceans: Their Physics, Chemistry, and General Biology. Prentice Hall, Inc., Englewood Cliffs, New Jersey, 1087 pp.

Taft B. A., S. P. Hayes, G. E. Friederich and L. A. Codispoti. 1991. Flow of abyssal water into the Samoa Passage. Deep-Sea Res., *38,* Suppl. 1, S103–S128.

Turner, J. S. 1973. Buoyancy Effects in Fluids. Cambridge University Press, Cambridge, England, 368 pp.

U.S. WOCE Implementation Plan. 1992. U.S. WOCE Implementation Report No. 4. U.S. WOCE Office, College Station, TX, 110 pp.

Warren, B. A. 1973. Transpacific hydrographic sections at Lats 43S and 28S; the SCORPIO Expedition-II. Deep water. Deep-Sea Res., *20*, 9–38.

Worthington, L. V. 1981. The water masses of the World Ocean: Some results of a fine-scale census, *in* Evolution of Physical Oceanography, B. A. Warren and C. Wunsch, eds., The MIT Press, Cambridge, Massachusetts, 42–69.